ACS APPLIED MATERIALS & INTERFACES

Research Article

www.acsami.org

Resistive Switching Induced by Metallic Filaments Formation through Poly(3,4-ethylene-dioxythiophene):Poly(styrenesulfonate)

Zhishun Wang, Fei Zeng,* Jing Yang, Chao Chen, and Feng Pan*

Laboratory of Advanced Materials (MOE), Department of Materials Science and Engineering, Tsinghua University, Beijing 100084, China

Supporting Information

ABSTRACT: We report the design and fabrication of Al/poly(3,4-ethylene-dioxythiophene):poly(styrenesulfonate) (PEDOT:PSS)/Cu resistive memory devices that utilize the Cu redox reaction and conformational features of PEDOT:PSS to achieve resistive switching. The top Cu electrode acts as the source of the redox ions that are injected through the PEDOT:PSS layer during the forming process. The Cu filament is confirmed directly using the cross-sectional images of transmission electron microscopy and energy-dispersive X-ray spectroscopy. The resultant resistive memory devices can operate over a small voltage range, i.e., the switching-on threshold voltage is less than 1.5 V and the absolute value of the switching-off threshold voltage is less than 1.0 V. The on/off current ratio is as large as 1×10^4 and the two different resistance states can be maintained over 10^6 s. Moreover, the devices present good thermal stability that the resistive switching can be observed even at temperature up to 160 °C, at which the oxidation of the Cu top electrode is the failure factor. Furthermore, the cause of failure for Al/PEDOT:PSS/Cu memory devices at higher temperature is confirmed to be the oxidation of Cu top electrode.

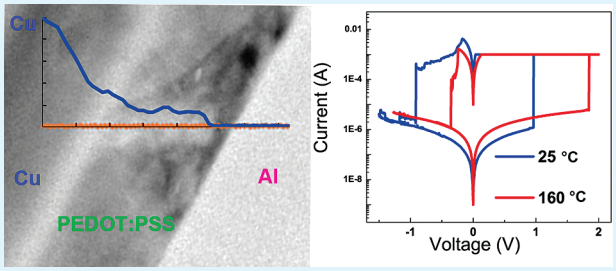

KEYWORDS: *PEDOT:PSS, nonvolatile, RRAM, switching voltage, metal filament, thermal stability*

INTRODUCTION

Resistance random access memory (RRAM), which features the advantages of a simple structure, high data density and low power consumption, is a potential candidate for next-generation nonvolatile memory applications.[1−4] A large variety of inorganic, organic, and polymeric materials show resistive switching (RS) behaviors.[4−7] Among them, polymeric materials have attracted much interest because of their easy processability, good environmental stability, and low cost. Several RS mechanisms have been proposed for different polymeric RRAM systems of which the conductive filament is regarded as the most attractive option to theoretically support the highest integration density.[7] Some conductive filament-based RRAM devices, which consist of inorganic materials, have realized memory elements with sizes below 100 nm, good stability, and high yield.[8,9] There are generally two types of conductive filaments for polymeric RRAM systems. One is a molecular filament related to the oxidation and reduction of conductive molecules.[10] This mechanism involves charge transport and accounts for the RS process in most polymer-based RRAM devices. Another type of conductive filament is a metal filament that is involved in ion redox in the semiconductor layer. It is hard to anticipate which mechanism will predominate in the future. Ion redox-based RRAM devices have many advantages such as ultrafast write/erase speed,[3] low switching voltage, long retention time, and good thermal stability at high temperatures.[11−14] These features are especially important for RRAM devices that depend on electrical input and output because lowering their power consumption and enhancing their speed and density are ultimate targets to enable the use of RRAM devices as core elements in next-generation computers. Therefore, scientists and engineers have great interest in obtaining the redox reaction of mobile ions in polymers because lowering power consumption and enhancing retention is pressing. An atomic switching effect was recently achieved by mixing polyethylene oxide (PEO) with silver perchlorate as the middle layer and using Ag as the top electrode (TE).[12] Because metal ions easily induce shortcut and failure in polymer, this work indicated the possibility and rationality to realize metal filament and enhance its controllability in polymer-based RRAM. However, the formation, distribution, shape, and composition of metal filament for this type of RRAM is still unclear. The process and position of formation and rupture of conducting paths are also ambiguous. This will bring difficulty in enhancing and modulating properties of the devices. On the basis of the above considerations, we try to find other polymer materials and fabricate corresponding RRAM devices depending on metal filament, and to determine the formation mechanism of the metal filament.

As we mentioned above, polymers have significant flexibility in their molecular design and synthesis. Thus, it is possible to utilize the intrinsic structure of a polymer to fabricate ion

Received: October 31, 2011
Accepted: December 15, 2011
Published: December 27, 2011

redox- or metal filament-based RRAM devices. We noticed that poly(3,4-ethylenedioxythiophene): poly(styrenesulfonate) (PEDOT:PSS) has a special conformation that is favorable for this image. PEDOT:PSS is a conductive polymer with environmental stability and easy processability and it has been widely used in many fields of organic electronics. As we know, PEDOT is a type of intrinsic conducting molecule and is the main functional part of PEDOT:PSS, while PSS is used for charge balance and solubility enhancement.[15] Groenendaal et al. identified early on that this structure enhances the redox properies of PEDOT:PSS.[16] The effect of metal ions when they interact with PEDOT:PSS is obvious. For example, a bivalent ion could cross-link PEDOT:PSS particles by electrostatic interactions.[17] Besides, PEDOT:PSS has the same heteroatom (S) as poly(3-hexyl thiophene) (P3HT), which is in favor of distributing Cu or Ag ions throughout the polymer layer.[14] Thus, it is possible to inject metal ions into PEDOT:PSS and form conductive filaments depending on ion redox. In this work, we used a Cu top electrode (TE), which can easily form sulfur or oxygen compounds with low activation energy.[18]

Memory devices based on PEDOT:PSS have been studied for many years. The first write-once-read-many-times (WORM) memory device based on PEDOT:PSS was fabricated early in 2003.[10] The bipolar and nonpolar RS behaviors in RRAM systems with ITO/PEDOT:PSS/Al, Au/PEDOT:PSS/Au and Al/PEDOT:PSS/Al structures were reported subsequently.[19−21] Recently, de Ruiters et al. reported that PEDOT is able to store up to five different memory states, and could therefore be utilized as a memory element to store multivalued digits in a single assembly.[22] These studies indicate that there is significant attention on PEDOT:PSS, which is a potential element for memory applications.[10,19−22] The major opinion on the RS mechanism in PEDOT:PSS-based RRAM devices is that oxidation and reduction occurs in the PEDOT:PSS film; this is accompanied by the formation and rupture of $PEDOT^+$ filaments.[10,19−21,23] Yet the influence needed to be clarified and considered in detail for the oxide layer existing possibly at the organic−inorganic interface as pointed out in refs 2 and 4. Therefore, the structural design of RRAM devices based on polymers including PEDOT:PSS previously focused on adjusting the energy level alignment at the interface of the metal−organic semiconductor. The aim was to control the injection of holes or electrons. In this paper, we first designed and fabricated RRAM devices with a Al/PEDOT:PSS/Cu structure and successfully injected Cu atoms into PEDOT:PSS to obtain Cu ion redox-based conductive filaments. Consequently, it was observed that the switching voltages were significantly reduced and the retention time was elongated to 1×10^6 s. Moreover, the RS behavior was still observed even at temperatures up to 160 °C.

EXPERIMENTAL DETAILS

Materials. PEDOT:PSS water based solution was purchased from Sigma-Aldrich Co. Ltd. and used as it is. The PEDOT and PSS contents are 0.5 and 0.8 wt %, respectively. Besides, the bandgap of PEDOT:PSS is 1.6 eV. The upper part of Figure 1 shows the chemical structures of PEDOT and PSS.

Fabrication of the Al/PEDOT:PSS/Cu Memory Devices. The lower part of Figure 1 shows a schematic configuration of the memory device based on Si/Al/PEDOT:PSS/Cu structure. A 150 nm Al BE was deposited by dc magnetron sputtering on a Si (111) substrate at room temperature. The PEDOT:PSS water-based solution (1.3 wt %) was then spin-coated and heated in a nitrogen-filled glovebox (O_2, H_2O < 1 ppm). Before spin-coating, the PEDOT:PSS aqueous solution was filtered through a membrane microfilter with a pore size of 0.45 μm. The filtered PEDOT:PSS solution was spin-coated onto Si/Al at 500 rpm for 10 s and then at 5000 rpm for 15 s. The thickness of the PEDOT:PSS film was determined to be ∼70 nm using a surface profiler (Veeco Dektak 150). After spin-coating, the PEDOT:PSS film was heated at 120 °C for 10 min in an inert atmosphere glovebox. Finally, a 100 nm Cu TE was prepared by DC magnetron sputtering. Cu TE was patterned using a shadow mask with a diameter ranging from 300 to 10 μm. Scanning electron microscopy (SEM) was applied to obtain the cross-sectional image and surface morphology of the Al/PEDOT:PSS/Cu memory devices.

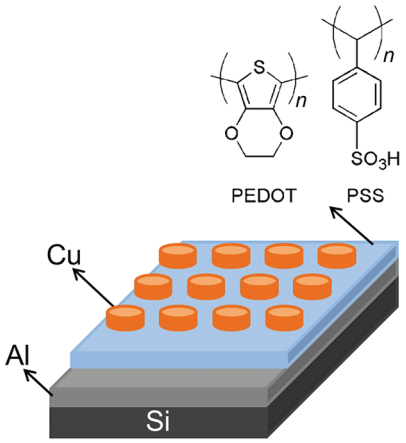

Figure 1. Schematic of the memory device with the Si/Al/PEDOT:PSS/Cu structure and the chemical structures of PEDOT and PSS.

Measurement. The electrical characterizations were performed on an Agilent B1500A semiconductor device analyzer under ambient conditions without any encapsulation. Voltages were applied to the Cu TE and the Al BE was grounded for all measurements in this report. During the electrical measurements, the memory devices were put on a Cascade M150 measurement platform, which can be heated to 300 °C. The cross section of Si/Al/PEDOT:PSS/Cu, which has been applied voltage and set to low resistive state, is analyzed using high resolution transmission electron microscopy (TEM) and energy-dispersive X-ray spectroscopy (EDX) on Tecnai F20 facility. The variation of surface valence and concentration after heating is analyzed using X-ray photoelectron spectroscopy (XPS) on a PHI quantera surface analysis equipment. The glass transition temperature (T_g) and degradation temperature (T_d) of PEDOT:PSS were also measured. During the measurements, PEDOT:PSS powder, which was obtained from the PEDOT:PSS water-based solution, was used. The preparation process is as follows. The PEDOT:PSS solution was heated in a drying oven at 90 °C to obtain the PEDOT:PSS powder. Then, the PEDOT:PSS powder was ground in an agate mortar for an hour. Finally, the ground PEDOT:PSS powder was heated in a vacuum chamber at 80 °C for 24 h. The T_g of PEDOT:PSS was measured in the range of ∼40−250 °C using DSC (model 2910). During the DSC analysis, dry nitrogen gas was purged at a flow rate of 50 mL/min and a ramping rate of 10 °C/min was employed. The T_d of PEDOT:PSS was measured in the range of 40−600 °C using TGA (model 2050). During the TGA analysis, dry nitrogen gas was purged at a flow rate of 25 mL/min and a ramping rate of 10 °C/min was employed.

RESULTS AND DISCUSSION

Initially, the devices were in the high resistance state (HRS), which may be induced by interfacial barrier, interfacial oxide, or reduction state of PEDOT. A high-voltage (>3 V) forming process (electroforming) was required to initially activate the RS behavior, as shown in Figure 2a. During the forming process, a current compliance of 1 mA was required to prevent breakdown of the memory devices. This kind of forming

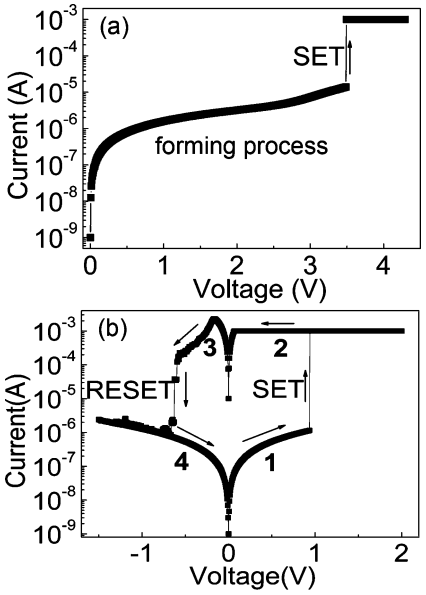

Figure 2. (a) The high-voltage forming process with a current compliance of 1 mA. (b) Typical $I-V$ curve for the devices after electroforming. The current is plotted in a semilogarithmic scale.

process has also been reported for many other RRAM systems.[11,12,24,25] Figure 2b shows the typical current−voltage ($I-V$) hysteresis after the forming process. In step 1, the voltage was scanned from 0 to 2.0 V and an abrupt increase in the current occurred at the voltage of 0.94 V, which is called the SET process. During the SET process, a current compliance of 1 mA was also required. We define V_{SET} as the switching-on threshold voltage for the SET process, which can function as a writing process for RRAM. In step 2, the voltage was scanned back from 2.0 to 0 V during which the device remained in the low resistance state (LRS). In step 3, while sweeping the voltage to −0.6 V, an opposite RESET process, which can function as an erasing process for RRAM, was observed. We therefore define V_{RESET} as the switching-off threshold voltage for the RESET process. In step 4, the memory devices remained in the HRS when the voltage was scanned back from −1.5 to 0 V. The Al/PEDOT:PSS/Cu memory devices were found to operate in an electrically bipolar switching mode. The values of V_{SET} and V_{RESET} after forming are different in every cycle, but they vary below a small voltage value, respectively. That is, $V_{SET} < 1.5$ V and $|V_{RESET}| < 1$ V. These values were notably lower than those of previous PEDOT:PSS and most polymer-based RRAM systems.[4,5,10,19−21] Such small switching voltages are applicable in low-power-consumption memory devices.

To examine the switching mechanism in Al/PEDOT:PSS/Cu memory devices, we investigated the previous $I-V$ curves with a log−log scale, in which the slope of fitted line contains the transport mechanism for both ON and OFF state. Figure 3a shows the double logarithmic plot and its linear fitting of the $I-V$ curve shown in Figure 2a (forming process). At low voltage, the log I−log V curve has a linear region with a slope of 1.0. At voltages higher than 2.8 V, the log I−log V curve has a region of steep current increase with a slope of ∼4.0. In classical trap-controlled space charge limited conduction (SCLC), which is a theoretical treatment of carrier injection into an insulator, the total current that flows in an insulator is determined by the electric field (drift current) and presence of carrier concentration gradients (diffusion current).[26] The typical slope of log I−log V curve is about 2.0 for SCLC mechanism in high voltage. The high voltage forming process above satisfactorily fits the strong space charge limited conduction (SCLC) mechanism,[3,21] according to the Child's Law in the presence of shallow trapping.[26] Figure 3b shows the log I−log V curve in Figure 2b and its linear fitting for the devices after electroforming. However, we did not observe significant SCLC phenomena. As can be seen from Figure 3b, the log I−log V curve in the HRS has a linear region with a slope of 1.0 at low voltage. At voltages higher than 0.3 V, the log I−log V curve is mostly linear with a slope of ∼1.2. The conduction mechanism in the HRS shown in Figure 3b changed from the strong SCLC effect to a weak SCLC effect after the forming process. We speculate that this is possibly caused by the low switching voltages within which the RS behavior occurs before the conduction behavior enters the strong SCLC region. The current is bypassed by the metal filament and then weak charge accumulation occurs. Meanwhile, we examined the current dependence of the voltage in the LRS, as shown in Figure 3b. A slope of 1.0 is observed in the LRS, which clearly shows Ohmic conduction behavior. The RS behavior after forming is obviously different from that in previously reported PEDOT:PSS-based RRAM devices,[4,5,10,19−21] and is difficult to ascribe to the redox reaction of PEDOT.

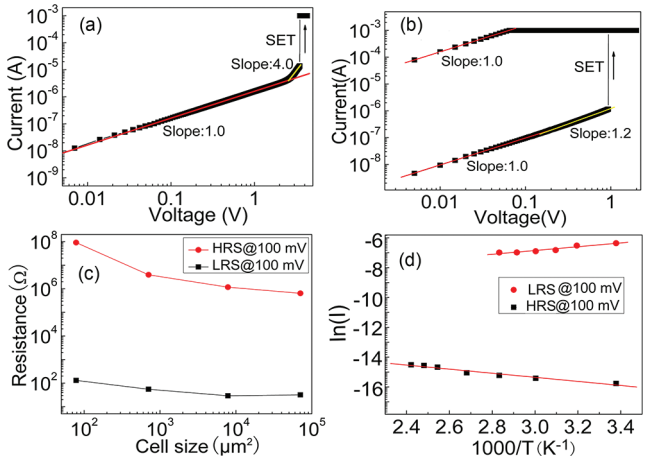

Figure 3. Double logarithmic plots and their linear fitting of the $I-V$ curves (a) in the forming process (Figure 2a) and (b) in the positive voltage sweep region for the devices after electroforming. (c) Cell size dependence of the resistances in the HRS and LRS. (d) Temperature dependence of the currents in the HRS and LRS.

Furthermore, we studied the dependence of the device resistance on cell size (Figure 3c). When the diameter of the Cu TE decreases from 300 to 10 μm, the resistance in the LRS (R_{LRS}) increases from 31.6 to 130.7 Ω, whereas the resistance in the HRS (R_{HRS}) increases from 6.4×10^5 to 9.1×10^7 Ω. R_{HRS} exhibits a stronger dependence on the cell size indicating that currents flow through the whole cell area in the HRS. In contrast, the small dependence of R_{LRS} on the cell size indicates that the conducting path in the LRS is localized.[27,28] In addition, the temperature dependence of the currents in the LRS and HRS was studied. Figure 3d shows the Arrhenius plot of the currents in the LRS and HRS. In the LRS, the current shows a negative dependence on temperature, which is a feature of a metallic conduction mechanism.[3,27] In contrast, the current shows a positive dependence on temperature when the memory devices are in the HRS, which implies a thermally

dx.doi.org/10.1021/am201518v | ACS Appl. Mater. Interfaces 2012, 4, 447−453

activated mechanism is functional.[3,27,29] The conduction mechanism in HRS might consist of hoping conduction between molecules, oxides, and Cu islands.

The dependences of R_{HRS} and R_{LRS} on cell size and temperature demonstrate clearly that the metal ion redox reaction occurred during the RS process. Considering that Al oxides are much more stable than Cu sulfides or oxides,[18,30] we determined that the RS mechanism involves the formation and rupture of the Cu filaments, i.e., a redox-controlled Cu bridge creation and rupture process. To verify the existence of Cu filament, we analyze the cross-sectional TEM image of a memory cell in LRS and corresponding EDX spectrum of Cu (Figure 4). We can see clearly a filament within PEDOT:PSS in

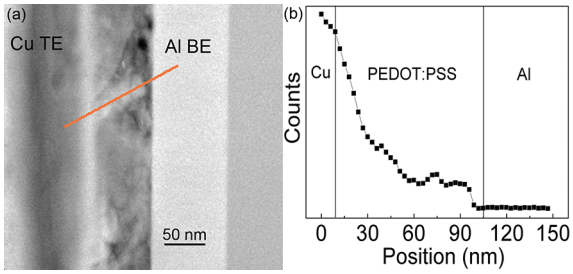

Figure 4. (a) Cross-sectional TEM images of memory cells in LRS. (b) EDX spectrum for Cu element profiles along the dotted lines marked in a.

Figure 4a. The length is about 70 nm and the diameter is about 7.6 nm. The filament connects robustly with Cu TE and extends to Al BE. However, it does not connect to Al BE as shown in both cross-sectional image and EDX spectrum. We also observed another similar cross-sectional image (not shown in Figure 4). We think that this might be due to the stress-induced separation during the preparation of TEM sample. This also gives hints of weak connection between the filament and the Al BE. On the basis of the observation of Figure 4, the RS behavior in Al/PEDOT:PSS/Cu memory devices can be explained by filament switching from formation and rupture of Cu filaments, namely, a redox-controlled Cu bridge creation and rupture process. When positive voltages are applied on Cu TE, oxidation occurs on this electrochemically active electrode. Therefore Cu ions are generated and dissolved into PEDOT:PSS middle layer through the Cu TE-PEDOT:PSS interface. In such a case, Cu TE serves as a source of Cu ions. With the external electric field, Cu ions will drift through the PEDOT:PSS middle layer toward Al BE. At Al BE, Cu ions are reduced into Cu atoms, which leads to growth of Cu filaments from the Al BE-PEDOT:PSS interface. As more Cu atoms congregate, Cu filaments grow longer and thicker, and finally connect Cu TE and Al BE. The formation of Cu filaments through metal-PEDOT:PSS interfaces and PEDOT:PSS middle layer drive the memory devices to switch to the LRS and induce Ohmic conduction behavior in the LRS, which is similar to the formation of Ag filaments observed in Pt/ZnO/Ag memory devices.[3,31] When negative voltages are applied on Cu TE, Cu atoms of some thin and weak sites of Cu filaments will be ionized, resulting in the rupture of whole filaments. Once the filaments are ruptured, the memory devices transfer from the LRS to the HRS. Consequently, the RS mechanism in Al/PEDOT:PSS/Cu memory devices can be described by the following formula:

$$Cu^{n+} + ne^{-} = Cu \ (n = 1 \text{ or } 2)$$

A similar formation and rupture of the Cu filaments were also discussed for AlN,[29] poly(3-hexyl thiophene)-,[13,14] and copper thiocyanate-based RRAM devices.[32] The redox-based switching during the forming process is a slow process, which includes the formation of a whole filament and requires high voltage. However, the switching after the forming process is a relatively fast process, during which filaments connect or rupture only at local point. It is still difficult to determine the exact rupture position of the Cu filaments from Figure 4 as well as that illustrated in other works.[31,33] Recent experiments show that metallic nanowires breakdown occurs near the two electrodes due to the stress induced by electromigration.[34] These results might support observations of ours and Figure 3c in ref 29, but cannot be used to judge whether the rupture position is at the TE or at the BE yet. In metal-filament-based RRAMs, the metal filament is surrounded by the semiconducting media, which acts as electrolyte in many times, so that the redox mechanism of metallic ions is still in the first consideration

To evaluate the reliability of the Al/PEDOT:PSS/Cu memory devices, their cycling endurance and retention time were both investigated. Figure 5a presents the cycling

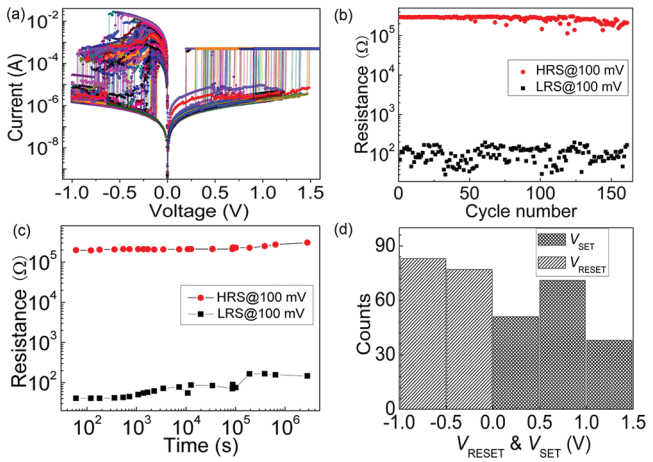

Figure 5. (a) Cycling endurance of the RS characteristics in a DC sweeping mode. (b) Distribution of R_{HRS} and R_{LRS} values during the cycling endurance test. (c) Retention time of the devices. (d) Statistical values of V_{SET} and V_{RESET} during the cycling endurance test.

endurance of the RS characteristics in a DC sweeping mode. As can be seen from Figure 5b, there is little degradation of the two stable resistance states over more than 150 switching cycles. Then we tested the stability of the memory devices. One cell was cycled and set to LRS and another to HRS. Then the resistance values of these two cells were read at 100 mV with time going. Figure 5c shows that the two resistance states are stable for $>1 \times 10^6$ s (>32 days) without serious deterioration, which is much longer than in other PEDOT:PSS-based RRAM devices.[10,19,20] Figure 5d shows the statistical values of V_{SET} and V_{RESET} during the cycling endurance test. It is evident that all the RESET processes occur in the voltage range of 0 to −1 V and all the SET processes occur below 1.5 V. These values of V_{SET} and V_{RESET} are significantly lower than the majority of corresponding values for molecular- or metal filament-based RRAM devices.[3−5,10,13,14,19−21]

From panels b and c in Figure 5, it is evident that, in most cases, R_{LRS} remains ∼50 Ω. If it is assumed that the metal

dx.doi.org/10.1021/am201518v | ACS Appl. Mater. Interfaces 2012, 4, 447−453

filament is a straight rod connecting two electrodes and that only a single filament is formed each time, the diameter of the metal filament can be estimated from the equation $R = \rho L/A$, where ρ, L, and A are the resistivity, length, and cross-sectional area of the metal filament, respectively.[13] In this case, considering the resistivity of Cu (1.7×10^{-8} Ω m) and the length of the filament (75 nm), the diameter of the Cu metal filament is calculated to be 4.1 nm. Because we have found a conductive filament with diameter of about 7.6 nm in Figure 4a, we think that the effective attachment to BE is quite limit for one metal filament. Thus, multiple conductive filaments always exist for metal filament type RRAM devices. Cho et al. have used conducting atomic force microscopy to get current images of conductive filament recently.[31] This method might be more effective to evaluate the distribution and diameters of the conducting paths. Whatever, our work provides the prospect of scaling the present polymer based RRAM devices down to the sub-100 nm range.

Although many PEDOT:PSS- and other polymer-based RRAM devices have been explored, little attention was given to enhancing their thermal stability, which is crucial for future applications. Thus, we studied the thermal stability of our Al/PEDOT:PSS/Cu RRAM devices (Figure 6a). The $I-V$ curves

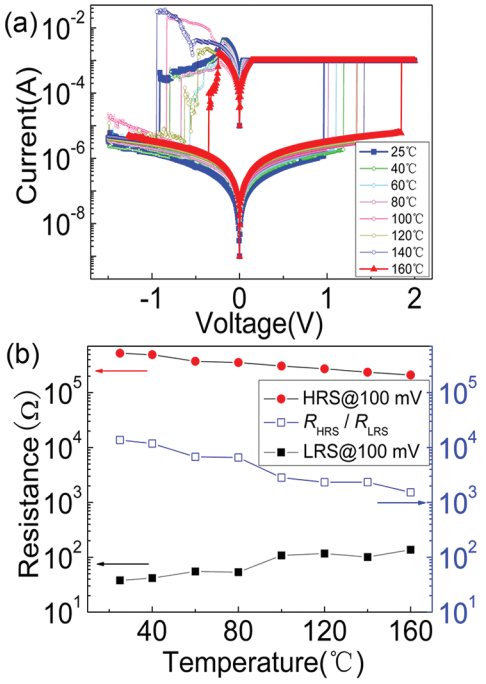

Figure 6. (a) $I-V$ curves of the Al/PEDOT:PSS/Cu memory devices when they are heated from 25 to 160 °C. (b) The values of R_{HRS}, R_{LRS}, and the switching window as a function of temperature.

were measured under ambient conditions in the temperature range of 25−160 °C. RS behavior was observed even when the temperature reached 160 °C. In addition, the values of R_{HRS} and R_{LRS} were measured when the memory devices were heated. Figure 6b shows the values of R_{HRS}, R_{LRS}, and the switching window as a function of temperature. It is evident that R_{HRS} and R_{LRS} are well separated with an effective switching window of $>1 \times 10^3$ up to 160 °C. The behaviors of these devices at high temperature are comparable to the recently reported RRAM devices based on poly(3,3′-di(9-anthracenemethoxy)-4,4′-biphenylene hexafluoroisopropylidenediphthalimide).[35]

When the devices were further heated to a temperature of 180 °C, they could be switched to the LRS when positive voltages were applied. However, the LRS could not be maintained. If the probe tip was reset to form a deeper contact with the Cu TE, the memory devices switched to the LRS again. The color of the Cu TE also changed when the devices were heated to 180 °C. Therefore, we speculated that the Cu TE might be oxidized when the memory devices were heated to 180 °C. Figure 7a shows the cross-sectional SEM image of the

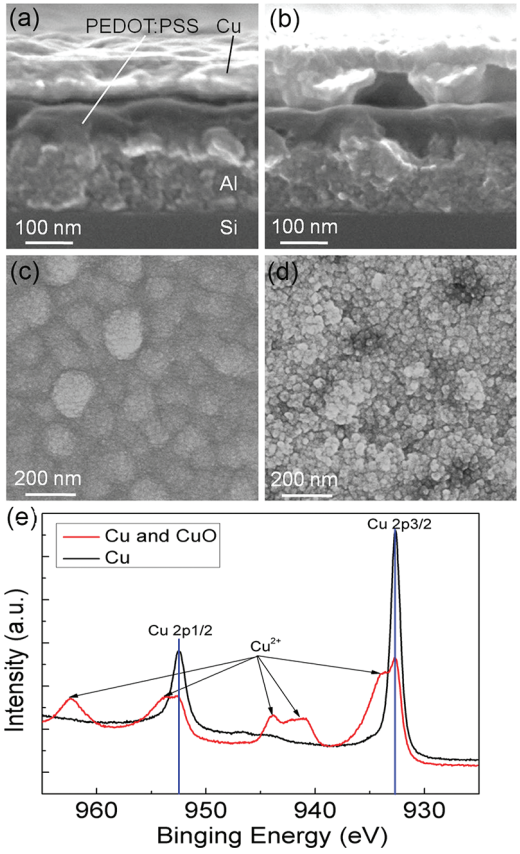

Figure 7. Cross-sectional SEM image of the memory device (a) at 25 °C and (b) after being heated at 180 °C. Surface SEM image of the memory device (c) at 25 °C and (d) after being heated at 180 °C. (e) Surface XPS spectra of the Cu TEs at 25 °C (black line) and after being heated at 180 °C (red line).

devices before and after heating. We found that the Cu TE cracked in some extent (Figure 7b) and its grain size became smaller (Figure 7d), which indicates that the surface of Cu TE was oxidized. This is further determined by the examination using XPS spectra (Figure 7e), in which we clearly found that Cu^{2+} appears intensively after the sample was heated at 180 °C (Figure 7e, red line).

In addition, the glass transition temperature and thermal stability of PEDOT:PSS were measured under a nitrogen atmosphere[36] To avoid the influence of water, we carried out the differential scanning calorimeter (DSC) test using the "1st heating−rapid cooling−2nd heating" mode, as shown in Figure 8a. During the DSC test, no onset temperature for the glass transition was found in the DSC thermogram. Additionally, we found that the PEDOT:PSS powder did not show obvious

dx.doi.org/10.1021/am201518v | ACS Appl. Mater. Interfaces 2012, 4, 447−453

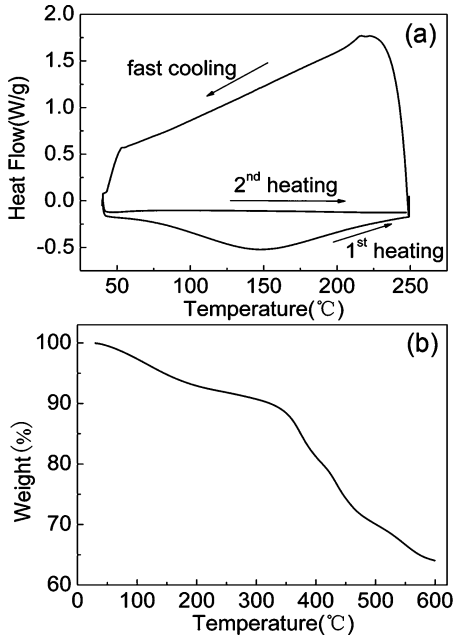

Figure 8. (a) DSC and (b) TGA thermogram of the PEDOT:PSS powder.

degradation below 300 °C, which indicates good thermal stability. The weight loss before 300 °C in the thermogravimetric analyzer (TGA) thermogram was cause by the evaporation of water. Therefore, it is concluded that PEDOT:PSS is thermally stable, and it is not PEDOT:PSS that induces the failure of our Al/PEDOT:PSS/Cu memory devices at 180 °C. From the above-mentioned discussion, we determined that it was the oxidation of the Cu TE that the LRS of the memory devices cannot be maintained when the memory devices were heated to 180 °C under ambient conditions. According to the experimental results shown in Figures 7 and 8, we used Pt to protect the Cu TE and observed robust RS behavior up to 200 °C (see Figure S1 in the Supporting Information). This result implies that proper protection and encapsulate will keep stability of Al/PEDOT:PSS/Cu devices.

CONCLUSION

We successfully designed and fabricated ion redox based-RRAM devices with the structure of Al/PEDOT:PSS/Cu. The Cu atoms from the Cu TE were injected into the PEDOT:PSS layer during the forming process. The RS mechanism results from the formation and rupture of a metal filament, which is based on the Cu redox reaction. The formation of Cu filament was confirmed by the cross-sectional TEM image of Al/PEDOT:PSS/Cu device at LRS. The devices can be operated over a small voltage range after the forming process, i.e., V_{SET} < 1.5 V and $|V_{RESET}|$ < 1 V, which is applicable for low power consumption memory. The effective switching window was as large as 1×10^4 and the two different resistance states can be maintained over 10^6 s. Moreover, the RS behavior is observed even when the memory devices are heated up to 160 °C indicating good thermal stability. Furthermore, PEDOT:PSS was proven to be a thermally stable material using DSC and TGA tests. The failure of the Al/PEDOT:PSS/Cu RRAM at higher temperatures is due to the oxidation of the Cu TE. Our work also provides flexibility for PEDOT:PSS applications in memory devices.

ASSOCIATED CONTENT

Supporting Information

I–*V* curves of the Al/PEDOT:PSS/Cu/Pt memory devices when they are heated from 25 to 200 °C. This information is available free of charge via the Internet at http://pubs.acs.org/.

AUTHOR INFORMATION

Corresponding Author

*Tel. +86-10-62795373 (F.Z.); +86-10-62772907 (F.P.). Fax: +86-10-62771160 (F.Z.). E-mail: zengfei@mail.tsinghua.edu.cn (F.Z.); panf@mail.tsinghua.edu.cn (F.P.).

ACKNOWLEDGMENTS

This work was supported by the National Basic Research Program of China (Grant 2010CB832905), National Hi-tech (Research and Development) Project of China (Grant 2007AA03Z426 and 2009AA034001), and the Program for New Century Excellent Talents in Universities (MOE).

REFERENCES

(1) Meijer, G. I. *Science* **2008**, *319*, 1625–1626.
(2) Waser, R.; Aono, M. *Nat. Mater.* **2007**, *6*, 833–840.
(3) Yang, Y. C.; Pan, F.; Liu, Q.; Liu, M.; Zeng, F. *Nano Lett.* **2009**, *9*, 1636–1643.
(4) Heremans, P.; Gelinck, G. H.; Muller, R.; Baeg, K. J.; Kim, D. Y.; Noh, Y. Y. *Chem. Mater.* **2011**, *23*, 341–358.
(5) Scott, J. C.; Bozano, L. D. *Adv. Mater.* **2007**, *19*, 1452–1463.
(6) Baek, S.; Lee, D. J.; Kim, J. Y.; Hong, S. H.; Kim, O.; Ree, M. *Adv. Funct. Mater.* **2007**, *17*, 2637–2644.
(7) Prime, D.; Paul, S. *Philos. Trans. R. Soc. London, Ser. A* **2009**, *367*, 4141–4157.
(8) Lee, M. J.; Lee, C. B.; Lee, D.; Lee, S. R.; Chang, M.; Hur, J. H.; Kim, Y. B.; Kim, C. J.; Seo, D. H.; Seo, S.; Chung, U. I.; Yoo, I. K.; Kim, K. *Nat. Mater.* **2011**, *10*, 625–630.
(9) Yang, J. J.; Pickett, M. D.; Li, X.; Ohlberg, D. A. A.; Stewart, D. R.; Williams, R. S. *Nat. Nanotechnol.* **2008**, *3*, 429–433.
(10) Moller, S.; Perlov, C.; Jackson, W.; Taussig, C.; Forrest, S. R. *Nature* **2003**, *426*, 166–169.
(11) Terabe, K.; Hasegawa, T.; Nakayama, T.; Aono, M. *Nature* **2005**, *433*, 47–50.
(12) Wu, S. M.; Tsuruoka, T.; Terabe, K.; Hasegawa, T.; Hill, J. P.; Ariga, K.; Aono, M. *Adv. Funct. Mater.* **2011**, *21*, 93–99.
(13) Joo, W. J.; Choi, T. L.; Lee, J.; Lee, S. K.; Jung, M. S.; Kim, N.; Kim, J. M. *J. Phys. Chem. B* **2006**, *110*, 23812–23816.
(14) Joo, W. J.; Choi, T. L.; Lee, K. H.; Chung, Y. S. *J. Phys. Chem. B* **2007**, *111*, 7756–7760.
(15) Kirchmeyer, S.; Reuter, K. *J. Mater. Chem.* **2005**, *15*, 2077–2088.
(16) Groenendaal, B. L.; Jonas, F.; Freitag, D.; Pielartzik, H.; Reynolds, J. R. *Adv. Mater.* **2000**, *12*, 481–494.
(17) Ghosh, S.; Rasmusson, J.; Inganis, O. *Adv. Mater.* **1998**, *10*, 1097.
(18) Sakamoto, T.; Sunamura, H.; Kawaura, H.; Terabe, K.; Hasegara, T.; Nakayama, T.; Aono, M. *Appl. Phys. Lett.* **2003**, *82*, 3032.
(19) Ha, H.; Kim, O. *Appl. Phys. Lett.* **2008**, *93*, 033309.
(20) Liu, X. H.; Ji, Z. Y.; Tu, D. Y.; Shang, L. W.; Liu, J.; Liu, M.; Xie, C. Q. *Org. Electron.* **2009**, *10*, 1191–1194.
(21) Wang, Z. S.; Zeng, F.; Yang, J.; Chen, C.; Yang, Y. C.; Pan, F. *Appl. Phys. Lett.* **2010**, *97*, 253301.
(22) de Ruiter, G.; Wijsboom, Y. H.; Oded, N.; van der Boom, M. E. *ACS Appl. Mater. Interfaces* **2010**, *2*, 3578–3585.
(23) Chia, P. J.; Chua, L. L.; Sivaramakrishnan, S.; Zhou, J. M.; Zhao, L. H.; Sim, W. S.; Yeo, Y. C.; Ho, K. H. *Adv. Mater.* **2007**, *19*, 4202–4207.
(24) Jo, S. H.; Lu, W. *Nano Lett.* **2008**, *8*, 392–397.

(25) Waser, R.; Dittmann, R.; Staikov, G.; Szot, K. *Adv. Mater.* **2009**, *21*, 2632−2663.
(26) Pope, M.; Swenberg, C. E. *Electronic Processes in Organic Crystals*; Clarendon/Oxford University Press: New York, 1982.
(27) Choi, H.; Pyun, M.; Kim, T. W.; Hasan, M.; Dong, R.; Lee, J.; Park, J. B.; Yoon, J.; Seong, D. J.; Lee, T.; Hwang, H. *IEEE Electron Device Lett.* **2009**, *30*, 302−304.
(28) Kim, T. W.; Choi, H.; Oh, S. H.; Jo, M.; Wang, G.; Cho, B.; Kim, D. Y.; Hwang, H.; Lee, T. *Nanotechnology* **2009**, *20*, 025201.
(29) Chen, C.; Yang, Y. C.; Zeng, F.; Pan, F. *Appl. Phys. Lett.* **2010**, *97*, 083502.
(30) Yang, Y. C.; Pan, F.; Zeng, F. *New J. Phys.* **2010**, *12*, 023008.
(31) Cho, B.; Yun, J. M.; Song, S.; Ji, Y.; Kim, D. Y.; Lee, T. *Adv. Funct. Mater.* **2011**, *21*, 3975−3981.
(32) Dong, Y. W.; Ji, X.; Xu, W.; Tang, J. Q.; Guo, P. *Electrochem. Solid-State Lett.* **2009**, *12*, H54−H57.
(33) Guo, X.; Schindler, C.; Menzel, S.; Waser, R. *Appl. Phys. Lett.* **2007**, *91*, 133513.
(34) Zhao, J.; Sun, H. Y.; Dai, S.; Wang, Y.; Zhu, J. *Nano Lett.* **2011**, *11*, 4647−4651.
(35) Park, S.; Kim, K.; Kim, D. M.; Kwon, W.; Choi, J.; Ree, M. *ACS Appl. Mater. Interfaces* **2011**, *3*, 765−773.
(36) Kim, D. M.; Park, S.; Lee, T. J.; Hahm, S. G.; Kim, K.; Kim, J. C.; Kwon, W.; Ree, M. *Langmuir* **2009**, *25*, 11713−11719.